RSC Advances




ROYAL SOCIETY OF CHEMISTRY

www.rsc.org/advances

# N-doped Porous Hollow Carbon Nanofibers Fabricated Using Electrospun Polymer Templates and Their Sodium Storage Properties

*Linchao Zeng, Weihan Li, Jianxiu Cheng, Jiaqing Wang, Xiaowu Liu, Yan Yu**

CAS Key Laboratory of Materials for Energy Conversion, Department of Materials Science and Engineering, University of Science and Technology of China, Anhui Hefei 230026, China

## Abstract

N-doped hollow porous carbon nanofibers (P-HCNFs) were prepared through pyrolyzation of hollow Polypyrrole (PPy) nanofibers that fabricated using electrospun polycaprolactone (PCL) nanofibers as sacrifice template. When used as anode material for NIBs, P-HCNFs exhibit a reversible capacity of 160 mAh $g^{-1}$ after 100 cycles at a current density of 0.05A $g^{-1}$. An improved rate capability is also obtained at even higher charge−discharge rate. When cycled at a current density of 2 A $g^{-1}$, the electrode still can release a reversible capacity of 80 $mAhg^{-1}$. The N-doped sites, one dimensional nanotube structure, and functionalized surface of P-HCNFs are capable of rapidly and reversibly accommodating sodium ions through surface adsorption and redox reactions. It is a promising anode material for next-generation NIBs.

**Keywords:** hollow nanofibers; N-doped; porous; sodium ion battery

## 1. Introduction

Owing to almost unmatched volumetric energy density, Li-ion batteries (LIBs) have dominated the portable electronics industry for the past 20 years.[1] However, the limited abundance of Li in the Earth's crust, its uneven geographic distribution and difficulties in recycling Li resources has raised concerns about large-scale application of LIBs.[2-4] Recently, Na-ion batteries (NIBs) have been considered as candidates for large-scale stationary energy storage, due to the advantages of sodium (e.g. high abundance, low cost, and very suitable redox potential (only 0.3 V above that of lithium).[2, 5-10] However, practical application of NIBs is greatly hampered by poor cyclability and low rate capability, which results from the poor kinetics of the Na ion de/insertion reaction caused by the relatively larger ionic radius (102 pm) of the Na cation than that of the Li cation (76 pm).[6, 11-14] Many efforts have been made to develop high performance NIBs, including cathodes, anodes, and electrolytes.[2, 5, 10, 15-24] The search of cathode materials for NIBs has proven to be fruitful, while the development of anode materials is still in their infancy.

Most of recently work focused on carbonaceous materials as anode for NIBs due to their large interlayer distance and disordered structure, which facilitates Na-ion insertion−extraction.[25-31] Firstly, Doeff et al. investigated the electrochemical insertion of sodium into a petroleum-coke carbon, observing a reversible capacity of 85 mAh/g.[32] Tirado's group studied the reversible insertion sodium in amorphous carbon black and delivered a capacity of 200 mAh/g considering only the discharge.[25] However, they only reported the results of few cycles. In order to further improve the electrochemical performance of carbonaceous materials anode, one approach is to tune their microstructure. Following this way, carbonaceous materials with various morphologies (nanofibers, nanotubes, nanospheres, nanosheets, carbon nanofoam) have been fabricated as anode for NIBs.[17, 20, 27, 28, 33] For instance, Tang et al. fabricated hollow carbon spheres as anode for NIBs, display a reversible capacity of 150 mAh/g.[20] Wang et al. demonstrated the use of 2D porous carbon sheets is an ideal high rate anode material for NIBs.[27, 34] Among those morphologies, one dimensional (1D) carbon nanostructure are considered to be attractive due to good

electronic conduction along the 1D nanostructure, short lithium ion diffusion distance, and high interfacial contact area with electrolytes.[17, 35, 36] In addition, the incorporation of N atom has been proven as another effective strategy to improve the electrochemical performance for the carbon-based Na-storage anodes.[34] Nitrogen as dopant to modify the carbon structures can generate extrinsic defects, hence improve capacity,[37] enhance surface wettability of the materials,[38] and increase electronic conductivity.[39] Therefore, many works using N-doped carbon materials as electrodes for NIBs have been reported.[34, 39, 40] However, these methods suffer from more or less severe drawbacks, such as the requirement of toxic precursors, using special instruments, and low yield. Therefore, the preparation of N-doped carbon materials by a simple, facile and scalable method is still a challenge.[41]

Electrospinning, as a simple, scalable, and versatile technique, has gained substantial attention in both academic research and industrial applications. It provides a straight forward and low-cost fabrication route to prepare 1D fiber with a diameter ranging from several tens of nanometers to a few micrometers.[42-44] In this work, we report the formation of N-doped hollow porous carbon nanofibers by carbonization-activation hollow PPy nanofibers using electrospun PCL fibers serve as sacrificial templates for subsequent in-situ polymerization of pyrrole coating on the fibers. As anode materials for NIBs, they exhibit high reversible capacity and good rate performance. It delivers a reversible capacity of 160 mAh/g after 100 cycles at 0.2C and excellent rate capability (~80 mAh/g at 8 C). The improved rate capability and cyclability can be attributed to the hollow porous structure and high-level N doping.

## 2. Experimental

### *2.1. Electrospinning of PCL nanofibers*

In a typical process of electrospinnig PCL (Mn=70,000~90,000, Aldrich) nanofibers, a solution of 1g PCL was dissolved in 10ml dichloromethane (DCM,99%, Aldrich ) that contained 0.0072g cetyltrimethylammonium bromide (CTAB, Aldrich). The obtained precursor solution was loaded into 10ml syringe with 19-gauge blunt tip

and the fibers were spun at about 15. 0 kV. The syringes were pushed by a syringe pump with a feeding rate of 4.02 ul.min$^{-1}$. The distance between tip of needle and the rotating cylinder was kept as 23 cm.

*2.2. Formation of hollow PPy nanofibers*

The obtained PCL nanofibers paper was cut in to several small pieces (6cm x 5cm). 10 pieces of nanofibers were immersed in 0.08 M aqueous solution of pyrrole (200ml). The polymerization of pyrrole (Py) and coating PPy on the PCL nanofibers at ice bath condition, which were initiated by dropping 0.07 M aqueous solution of $FeCl_3$ (200 ml) for 24 h with continuous stirring. The collected PCL (core)- PPy (sheath) fibers were washed with deionized water for several times to remove the residual $FeCl_3$. Subsequently, the PCL (core)-PPy (sheath) fibers were immersed in DCM for another 24 h to extract the PCL core and the hollow PPy nanofibers were obtained. Finally, the hollow PPy nanofibers were washed with deionized water several times to remove the DCM and dried in an oven at 80 ℃.

*2.3. Preparation of N-doped porous hollow carbon nanofibers (P-HCNFs)*

The porous hollow carbon nanofibers were synthesized by pyrolysis of hollow PPy nanofibers that were chemically activated with KOH before. Typically, a mixture of hollow PPy nanofibers (0.3 g) and KOH (0.9 g) (PPy: KOH=1:3, weight ratio) was added into 20 ml deionized water and then the mixture stirred for 12 h. Then the product was filtered and dried at 80 ℃ in an oven. After that the PPy was chemical activation at 700℃ with a heating rate of 3 ℃min$^{-1}$ and kept for 0.5h under nitrogen atmosphere. Then the product was washed with deionized water until the filtrate is neutral and dried in an oven at 80℃. Finally, the N-doped porous hollow carbon nanofibers (denoted as P-HCNFs) were obtained. The N-doped hollow carbon nanofibers (HCNFs) was prepared according to a similar treatment but without the activation procedure.

*2.4 Structural analysis and electrochemical measurements*

X-ray powder diffraction (XRD) patterns of the products were on a Philips X'Pert PRO SUPER X-ray diffractormeter with Cu $K_\alpha$ radiation. Filed-Emission Scanning electron microscopy (FESEM), transmission electron microscopy (TEM) and

high-resolution TEM (HRTEM) images were taken by a scanning electron microscopy (JEOL, Tokyo, Japan) and a transmission electron microscopy (JEOL, Tokyo, Japan), respectively, to study the morphology and microstructure of P-HCNFs and HCNFs. The Raman spectroscopy was used to study the degree of graphitization. An ASAP 2020 Accelerated Surface Area and Porosimetry instrument was used to measure the products' nitrogen adsorption/desorption isotherms. X-ray photoelectron spectroscopy (XPS) analysis was carried to investigate the nature of nitrogen species at the surface of P-HCNFs.

The working electrodes was prepared by mixing active material (here P-HCNFs or HCNFs) (90 wt%) and poly(vinylidene) fluoride (PVDF, 10wt%) in N-methyl-2pyrrolidone (NMP) to form a slurry, then coated on a copper foil, followed by drying at 80 $^{o}$C under vacuum overnight and cutting into pellets with a diameter of 14mm. The obtained discs were used as the electrodes of electrochemical cells P-HCNFs (or HCNFs) /Na with $NaClO_4$ (1 M) in propylene carbonate (PC) as the electrolyte. Glass fiber (Whatman) was used as a separator film. Pure sodium foil (99.9%, Aldrich) was used as counter electrode and reference electrode. The cells were assembled in an argon-filled glove box (MBRAUN LABMASTER 130) where both moisture and oxygen levels were kept below 1ppm. Electrochemical experiments were performed using coin cells (CR2032). The galvanostatic charge-discharge tests were carried out at a voltage interval of 0-2.8 V on a battery test system (Neware BTS-610). Cyclic voltammetry (CV) was conducted by using a CHI 660D electrochemical workstation at a scan rate of 0.2 mV/s (Chenhua Instrument Company, Shanghai, China).

## 3. Results and discussion

The processing steps of our fabrication procedure are shown schematically in Figure 1. The precursor solution of PCL-CTAB/DCM was electrospun into fibers (Fig. 1A). As shown in Fig. 1B, the in-situ polymerization reaction for PPy involved the use of $Fe^{3+}$ as an oxidant and $Cl^{-}$ as dopant. The CTAB was served as surfactant to self-assembled Py on PCL fibers.[45] Then the obtained PCL fibers were served as a

sacrificial template to create hollow PPy fiber. The hollow PPy fibers were subsequently chemically activated with KOH at $N_2$ atmosphere, resulting in N-doped porous hollow carbon nanofibers (P-HCNFs) with large surface areas.

Figure 2A shows the field emission scanning electron microscopy (FESEM) image of the as-electrospun PCL-CTAB fibers. The as-spun fibers display a continuous fibrous morphology with uniform diameter distribution. The inset image of Figure 2A shows that these nanofibers have smooth surface and an average diameter of ~ 300 nm. Figure 2B displays the FESEM image of PPy nanotubes after extraction the PCL cores by DCM. It can be seen from the broken part of the fiber that after dissolution of the PCL, a tubular structure was obtained. Obviously, PPy nanotubes replicating the morphology of the as-spun PCL fibers were produced. The surfaces of PPy nanotubes are rough. The outer diameter of the PPy nanotubes varied between approximately 500 and 800 nm. After activation with KOH under $N_2$ atmosphere, the PPy nanotubes maintained their nanotubes morphology and transformed into porous hollow carbon nanotubes (P-HCNFs) (Fig. 2C). The outer diameter of obtained P-HCNFs is about 500 nm, slightly less than the diameter of the PPy nanotubes, displaying a shrinkage that can be ascribed to the decomposition of organic components of PPy during the calcination step. Fig.2D reveals the morphology of HCNFs, showing a similar morphology with P-HCNFs.

The microstructure of P-HCNFs and HCNFs were further studied by transmission electron microscopy (TEM). Fig. 3A confirms the hollow structure of P-HCNFs. The inner diameter of P-HCNFs is ~ 370 nm and the wall thickness of P-HCNFs is about 65 nm. The HRTEM image of P-HCNFs (Fig. 3B) reveals that the large quantities of micropores are homogeneously distributed within HCNFs, indicating its amorphous structure. These micropores resulted from the loss of hydrogen and nitrogen in PPy and reaction between PPy and KOH during the carbonization process and can provide position to sodium ions for reversible accommodate.[34] Owing to these special structure characters, the material might have an excellent electrochemical performance when used as anode material for NIBs. Fig.3C shows the hollow structure of HCNFs. The HRTEM image in Figure 3D shows the formation

of porous carbon.

To further examine the surface and characterize the pore size of the P-HCNFs and HCNFs, the two samples were studied by nitrogen adsorption-desorption tests. Figure 4A and 4B exhibit type-IV nitrogen adsorption-desorption isotherms with H4-type hysteresis loop. The specific Brunauer-Emmett-Teller (BET) surface area of P-HCNFs and HCNFs are 868 $m^2$ $g^{-1}$ and 134 $m^2$ $g^{-1}$, respectively. Obviously the BET surface area of P-HCNFs is much higher than that of HCNFs. The inset of Fig. 4A and Fig. 4B are the pore size distribution of P-HCNFs and HCNFs, respectively. The P-HCNFs possess small micropores (peak at 1.27nm), and while the HCNFs possess both mesopores (peak at 2.52nm) and micropores (peak 1.59nm and 0.73nm).

X-ray photoelectron spectroscopy (XPS) is used to investigate the nature of nitrogen species at the surface of P-HCNFs and HCNFs. It has been demonstrated that PPy precursor has only one type of nitrogen atom named N-5 within a pentagonal ring.[46] However, three peaks at 398.2, 399.9, and 401eV can be observed to correspond pyridinic-N (N-6), pyrrolic-N (N-5) and graphite-N (N-Q) in the high-resolution N 1s peaks (Fig. 5A) after carbonization-activation of PPy with KOH.[34, 46]Obviously, during the carbonization-activation process, part of nitrogen atoms within the pentagonal ring of polypyrrole are converted into two types of nitrogen (N-6 and N-Q). It has been proved such nitrogen-containing species (pyridinic-N and graphite-N) can improve the electrochemical activity of nitrogen-doped carbon materials. [34] For HCNFs, such N 1s peaks are also observed (Fig. 5B).

The phase of P-HCNFs and HCNFs were checked by XRD (Fig. 6A). Two characteristic peaks of carbon appear at $2\theta = 25^{o}$ and $43^{o}$, corresponding to the (002) diffraction and (100) diffraction of hexagonal carbon material (JCPDS, Card No. 75-1621), respectively.[46] The two peaks' intensity of P-HCNFs are a little lower than that of HCNFs', suggesting a lower graphitic crystallinity of P-HCNFs, due to more graphene fragments and defects generate when KOH is added to chemical activation.[46] The Raman spectra of P-HCNFs and HCNFs (Fig. 6B) show two broad peaks at about 1580$cm^{-1}$ (G-band) and 1350$cm^{-1}$ (D-band), correspond to the $E_{2g2}$

graphitic mode and the defect-induced mode, respectively.[35] The disorder degree of the carbon is estimated by the index R ($R=I_D/I_G$).[47] The R value for P-HCNFs and HCNFs are 1.01 and 0.95, respectively. It indicates that the two materials are low degree of graphitization with a high disorder structure, which is in consistent with the XRD patterns and HRTEM results. [48]

The electrochemical performance of the P-HCNFs and HCNFs electrodes were evaluated by using a half-cell with sodium metal. Figure 7 shows cyclic voltammetry (CV) curves of the P-HCNFs and HCNFs in the range of 0-2.6 V. The sharp cathodic peaks (Fig. 7A) at 0.42 V of the first cycle, which is due to the decomposition of the electrolyte and the formation of solid electrolyte interface (SEI).[34, 49] This peak disappears after the first cycle due to the anode is isolated from the electrolyte after the formation of SEI in the 1st cycle. A pair of redox peaks near 0 V can be related to sodium ions insertion into/extraction out of the micropores.[2] During the subsequent cycles, the CV curves almost overlap which indicates the P-HCNFs display good capacity retention. In case of HCNFs (Fig. 7B), an irreversible peaks occurred at 0.97V during the reduction process in the first CV curve, which also can be ascribed to decomposition of electrolyte and the SEI formation. Additionally, a pair of small and broad redox peaks can be observed in a wide potential range of 0.2-1.2V, which is attributed to sodium ion insertion into hard carbon.

Fig. 8A and 8B show the charge/discharge profiles of the P-HCNFs and HCNFs electrodes at a current density of 0.05 A $g^{-1}$ (0.2C) in the voltage range of 0~2.8V. The initial discharge and charge capacities of P-HCNFs (Fig. 8A) are 993 and 319 $mAhg^{-1}$, respectively, showing a 32% initial Coulombic efficiency. The large irreversible capacity loss is caused by the decomposition of electrolyte and formation of SEI layer.[34, 49] The P-HCNFs electrode shows sloping voltage profile and an indistinct plateau near 0V in subsequent cycles, which result from sodium ion insertion into nanopores of hard carbon.[34] In case of HCNFs, the voltage profile also displays similar behavior. It delivers a discharge and charge capacity of 423 mAh $g^{-1}$ and 174 $mAhg^{-1}$, respectively, according an initial Coulombic efficiency of 41%. The improvement of initial Coulombic efficiency is related to the less formation of SEI. It

has been demonstrated that the lager contact surface area between the electrode and electrolyte will result in more SEI and higher initial capacity loss. [50]

Figure 8C compares the cycle performance of P-HCNFs and HCNFs electrodes at a current density of 0.05 A $g^{-1}$. Obviously, the cycling performance of P-HCNFs electrode is much better than HCNFs electrode. The P-HCNFs electrode retains a reversible capacity of 160 mAh $g^{-1}$ after 100 cycles, corresponding to 50.2% of the initial charge capacity. While for the HCNFs electrode, it only delivers a reversible capacity of 40mAh $g^{-1}$ after 100 cycles, corresponding to 22.4% of the initial charge capacity. To further illustrate the improvement of electrochemical performance of P-HCNFs, the rate capability of the both electrodes were investigated (Fig. 8D). The reversible capacity of P-HCNFs electrode are 190 mAh $g^{-1}$, 160 mAh $g^{-1}$, 120 mAh $g^{-1}$, 86 mAh $g^{-1}$, 80 mAh $g^{-1}$ and 80 mAh $g^{-1}$ when cycled at a current density of 0.05, 0.1, 0.25, 0.5, 1 and 2 A $g^{-1}$, respectively. After the current density was tuned back to 50 mA $g^{-1}$, the reversible capacity of P-HCNFs electrode also recovered to 180 mAh $g^{-1}$. It demonstrates excellent cycle stability. While for HCNFs electrodes, the rate capability is much worse. When cycled at 1 A $g^{-1}$, it only delivers a capacity of 4 mAh $g^{-1}$.

The improvement of electrochemical performance of P-HCNFs electrode can be explained as follows. i) The 1D nanotube structure can provide short ion transfer length and continuous electron transportation. Besides, the homogeneous distributed porous channels in P-HCNFs can enable effective short length for both sodium ions and electrons. ii) The nitrogen doping in P-HCNFs can improve the electrochemical reactivity and electronic conductivity of material.[51]

## 4. Conclusions

In summary, we fabricated N-doped hollow porous carbon nanofibers via a two-step method. First, the hollow Polypyrrole (PPy) nanofibers were fabricated via a combination of electrospinning and aqueous polymerization. Specifically, nanofibers electrospun from poly(ε-caprolactone) (PCL) employed as sacrificial template to generate hollow nanofibers of polypyrrole (PPy) via in situ polymerization. Second,

the obtained PPy nanotubes were carbonized and then further chemically activated with KOH to prepare the P-HCNFs. The P-HCNFs display hollow tubular structure and possess a surface area as high as 868 $m^2g^{-1}$. When used as an anode material for NIBs, the P-HCNFs electrode delivers a reversible capacity as high as 160 $mAhg^{-1}$ after 100 cycles at a current density of 0.05A g-1. The results demonstrate that the P-HCNFs are a promising candidate for the construction of low-cost sodium ion battery systems.

**Acknowledgements**

This work was financially supported by the National Natural Science Foundation of China (No.21171015, No.21373195), the "1000 plan" from Chinese Government, program for New Century Excellent Talents in University (NCET), the Fundamental Research Funds for the Central Universities (WK2060140014) and sofja kovalevskaja award from Alexander von Humboldt Foundation.

**References:**

[1] J.M. Tarascon, M. Armand, Nature, 414 (2001) 359-367.
[2] M.D. Slater, D. Kim, E. Lee, C.S. Johnson, Adv Funct Mater, 23 (2013) 947-958.
[3] H. Kim, D.J. Kim, D.-H. Seo, M.S. Yeom, K. Kang, D.K. Kim, Y. Jung, Chemistry of Materials, 24 (2012) 1205-1211.
[4] J.M. Tarascon, Nature chemistry, 2 (2010) 510.
[5] S. Komaba, W. Murata, T. Ishikawa, N. Yabuuchi, T. Ozeki, T. Nakayama, A. Ogata, K. Gotoh, K. Fujiwara, Adv Funct Mater, 21 (2011) 3859-3867.
[6] V. Palomares, P. Serras, I. Villaluenga, K.B. Hueso, J. Carretero-González, T. Rojo, Energy & Environmental Science, 5 (2012) 5884.
[7] S.-W. Kim, D.-H. Seo, X. Ma, G. Ceder, K. Kang, Advanced Energy Materials, 2 (2012) 710-721.
[8] B.L. Ellis, L.F. Nazar, Current Opinion in Solid State and Materials Science, 16 (2012) 168-177.
[9] Y. Kim, Y. Park, A. Choi, N.S. Choi, J. Kim, J. Lee, J.H. Ryu, S.M. Oh, K.T. Lee, Adv Mater, 25 (2013) 3045-3049.
[10] N. Yabuuchi, M. Kajiyama, J. Iwatate, H. Nishikawa, S. Hitomi, R. Okuyama, R. Usui, Y. Yamada, S. Komaba, Nat Mater, 11 (2012) 512-517.
[11] J. Qian, X. Wu, Y. Cao, X. Ai, H. Yang, Angewandte Chemie International Edition, 52 (2013) 4633-4636.
[12] V.L. Chevrier, G. Ceder, Journal of The Electrochemical Society, 158 (2011) A1011.
[13] Y. Cao, L. Xiao, W. Wang, D. Choi, Z. Nie, J. Yu, L.V. Saraf, Z. Yang, J. Liu, Adv Mater, 23 (2011) 3155-3160.
[14] F. Sauvage, L. Laffont, J.M. Tarascon, E. Baudrin, Inorganic Chemistry, 46 (2007) 3289-3294.

[15] R. Alcántara, M. Jaraba, P. Lavela, J.L. Tirado, Chemistry of Materials, 14 (2002) 2847-2848.
[16] J.F. Qian, M. Zhou, Y.L. Cao, X.P. Ai, H.X. Yang, Advanced Energy Materials, 2 (2012) 410-414.
[17] Y. Cao, L. Xiao, M.L. Sushko, W. Wang, B. Schwenzer, J. Xiao, Z. Nie, L.V. Saraf, Z. Yang, J. Liu, Nano Lett, 12 (2012) 3783-3787.
[18] L. Zhao, J. Zhao, Y.S. Hu, H. Li, Z. Zhou, M. Armand, L. Chen, Advanced Energy Materials, 2 (2012) 962-965.
[19] Y. Park, D.S. Shin, S.H. Woo, N.S. Choi, K.H. Shin, S.M. Oh, K.T. Lee, S.Y. Hong, Advanced Materials, 24 (2012) 3562-3567.
[20] K. Tang, L.J. Fu, R.J. White, L.H. Yu, M.M. Titirici, M. Antonietti, J. Maier, Advanced Energy Materials, 2 (2012) 873-877.
[21] A. Abouimrane, W. Weng, H. Eltayeb, Y. Cui, J. Niklas, O. Poluektov, K. Amine, Energy and Environmental Science, 5 (2012) 9632-9638.
[22] Y. Sun, L. Zhao, H. Pan, X. Lu, L. Gu, Y.S. Hu, H. Li, M. Armand, Y. Ikuhara, L. Chen, X. Huang, Nature communications, 4 (2013) 1870.
[23] A. Ponrouch, E. Marchante, M. Courty, J.M. Tarascon, M.R. Palacín, Energy and Environmental Science, 5 (2012) 8572-8583.
[24] T. Matsuda, M. Takachi, Y. Moritomo, Chemical Communications, 49 (2013) 2750-2752.
[25] R. Alcántara, J.M. Jiménez-Mateos, P. Lavela, J.L. Tirado, Electrochemistry Communications, 3 (2001) 639-642.
[26] R. Alcantara, F.J.F. Madrigal, P. Lavela, J.L. Tirado, J.M.J. Mateos, C.G. de Salazar, R. Stoyanova, E. Zhecheva, Carbon, 38 (2000) 1031-1041.
[27] Z.H. Wang, L. Qie, L.X. Yuan, W.X. Zhang, X.L. Hu, Y.H. Huang, Carbon, 55 (2013) 328-334.
[28] Y. Shao, J. Xiao, W. Wang, M. Engelhard, X. Chen, Z. Nie, M. Gu, L.V. Saraf, G. Exarhos, J.G. Zhang, J. Liu, Nano Letters, 13 (2013) 3909-3914.
[29] P. Thomas, J. Ghanbaja, D. Billaud, Electrochimica Acta, 45 (1999) 423-430.
[30] M. Dubois, D. Billaud, Electrochimica Acta, 47 (2002) 4459-4466.
[31] X. Xia, J.R. Dahn, Journal of The Electrochemical Society, 159 (2012) A515.
[32] M.M. Doeff, Y.P. Ma, S.J. Visco, L.C. Dejonghe, Journal of The Electrochemical Society, 140 (1993) L169-L170.
[33] S. Wenzel, T. Hara, J. Janek, P. Adelhelm, Energy and Environmental Science, 4 (2011) 3342-3345.
[34] H.G. Wang, Z. Wu, F.L. Meng, D.L. Ma, X.L. Huang, L.M. Wang, X.B. Zhang, ChemSusChem, 6 (2013) 56-60.
[35] L. Qie, W.M. Chen, Z.H. Wang, Q.G. Shao, X. Li, L.X. Yuan, X.L. Hu, W.X. Zhang, Y.H. Huang, Adv Mater, 24 (2012) 2047-2050.
[36] P. Thomas, D. Billaud, Electrochimica Acta, 46 (2000) 39-47.
[37] D. Hulicova-Jurcakova, M. Seredych, G.Q. Lu, T.J. Bandosz, Advanced Functional Materials, 19 (2009) 438-447.
[38] H. Guo, Q. Gao, Journal of Power Sources, 186 (2009) 551-556.
[39] B. Guo, X.G. Sun, G.M. Veith, Z. Bi, S.M. Mahurin, C. Liao, C. Bridges, M.P. Paranthaman, S. Dai, Advanced Energy Materials, 3 (2013) 708-712.
[40] D. Wei, Y. Liu, Y. Wang, H. Zhang, L. Huang, G. Yu, Nano Letters, 9 (2009) 1752-1758.
[41] L.F. Chen, X.D. Zhang, H.W. Liang, M. Kong, Q.F. Guan, P. Chen, Z.Y. Wu, S.H. Yu, Acs Nano, 6 (2012) 7092-7102.

[42] Y. Yu, L. Gu, C. Wang, A. Dhanabalan, P.A. van Aken, J. Maier, Angewandte Chemie International Edition, 48 (2009) 6485-6489.
[43] Y. Yu, L. Gu, C.B. Zhu, P.A. van Aken, J. Maier, J Am Chem Soc, 131 (2009) 15984-+.
[44] K. Tang, Y. Yu, X. Mu, P.A. van Aken, J. Maier, Electrochemistry Communications, 28 (2013) 54-57.
[45] J. Xie, M.R. MacEwan, S.M. Willerth, X. Li, D.W. Moran, S.E. Sakiyama-Elbert, Y. Xia, Adv Funct Mater, 19 (2009) 2312-2318.
[46] F. Su, C.K. Poh, J.S. Chen, G. Xu, D. Wang, Q. Li, J. Lin, X.W. Lou, Energy & Environmental Science, 4 (2011) 717.
[47] N.A. Kaskhedikar, G.L. Cui, J. Maier, V. Fedorov, V. Makotchenko, A. Simon, Zeitschrift Fur Anorganische Und Allgemeine Chemie, 637 (2011) 523-529.
[48] L. Ji, Z. Lin, A.J. Medford, X. Zhang, Carbon, 47 (2009) 3346-3354.
[49] Y. Mao, H. Duan, B. Xu, L. Zhang, Y. Hu, C. Zhao, Z. Wang, L. Chen, Y. Yang, Energy & Environmental Science, 5 (2012) 7950.
[50] M.E. Spahr, H. Buqa, A. Würsig, D. Goers, L. Hardwick, P. Novák, F. Krumeich, J. Dentzer, C. Vix-Guterl, Journal of Power Sources, 153 (2006) 300-311.
[51] Z.S. Wu, W.C. Ren, L. Xu, F. Li, H.M. Cheng, Acs Nano, 5 (2011) 5463-5471.

**Figure Captions**

**Fig. 1 A~B** Schematic illustration of the synthesis process for P-HCNFs.

**Fig. 2** FESEM micrographs of as-electrospun PCL-CTAB nanofibers (A), PPy nanotubes (B), P-HCNFs (C) and HCNFs (D). The inset pictures are corresponding high magnification images.

**Fig. 3** TEM image (A) and HRTEM image (B) of P-HCNFs. TEM image (C) and HRTEM image (D) of HCNFs.

**Fig. 4** Nitrogen adsorption-desorption isotherms and PSD (inset) of P-HCNFs (A) and HCNFs (B).

**Fig. 5** N1s XPS spectra of P-HCNFs (A) and HCNFs (B).

**Fig. 6** XRD patterns (A) and Raman patterns (B) of P-HCNFs and HCNFs.

**Fig. 7** Cyclic voltammograms of a P-HCNFs (A) and HCNFs (B) electrode between 0 and 2.6 V at a potential sweep rate of $1mVs^{-1}$.

**Fig. 8** Voltage profiles of P-HCNFs (A) and HCNFs (B) electrodes at a current density of 50 $mAg^{-1}$. (C) Cycle performances of P-HCNFs and HCNFs electrodes at a current density of 50 $mAg^{-1}$. (D) Discharge capacity of P-HCNFs and HCNFs electrodes as a function of charge-discharge cycles at different charge-discharge current densities of 0.05 (0.2 C), 0.1 (0.4 C), 0.25 (1 C), 0.5 (2 C), 1 (4C), 2 (8C) $Ahg^{-1}$, respectively.

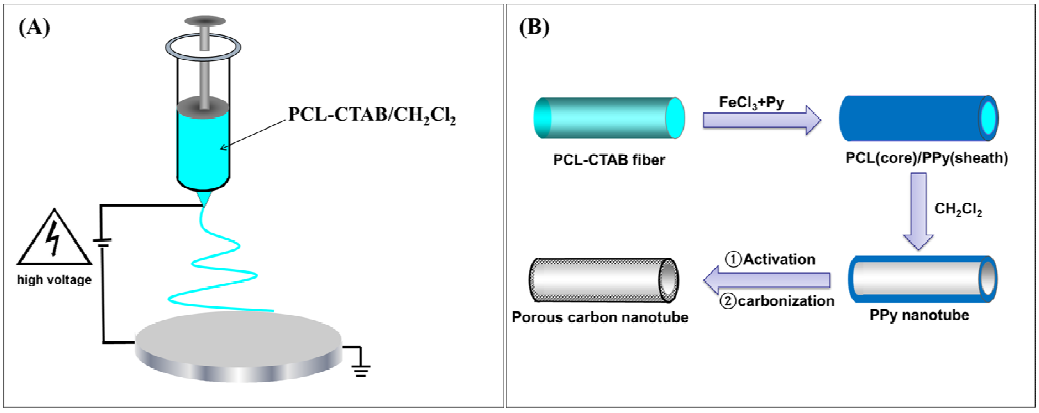


**Fig. 1**

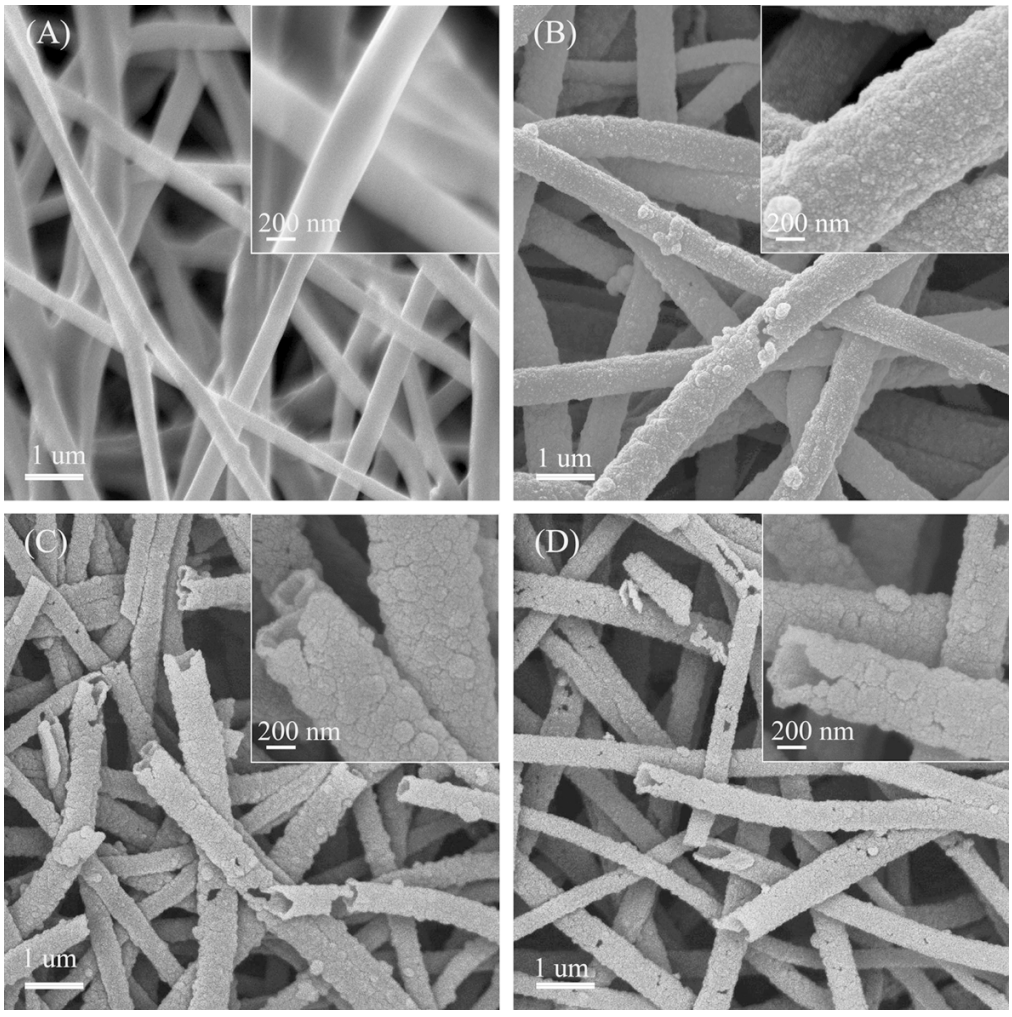


**Fig. 2**

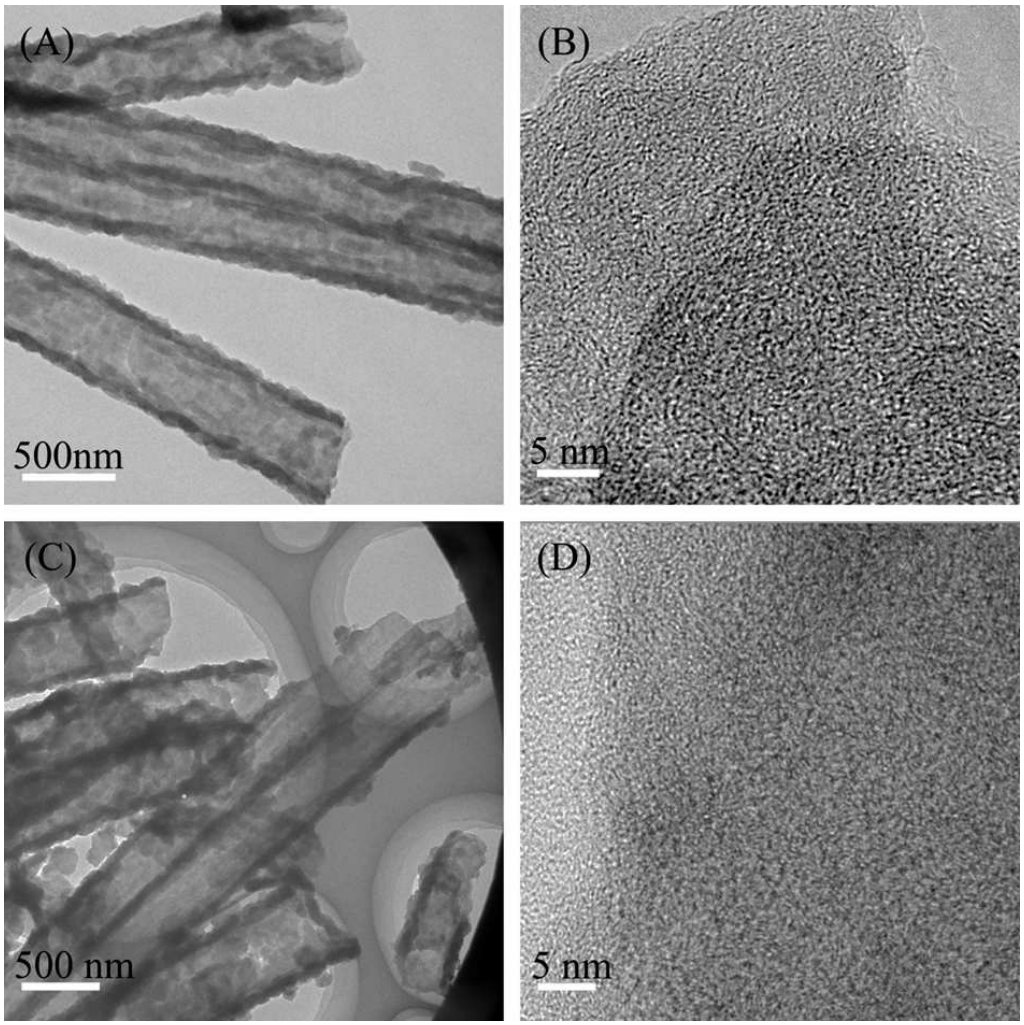


**Fig. 3**

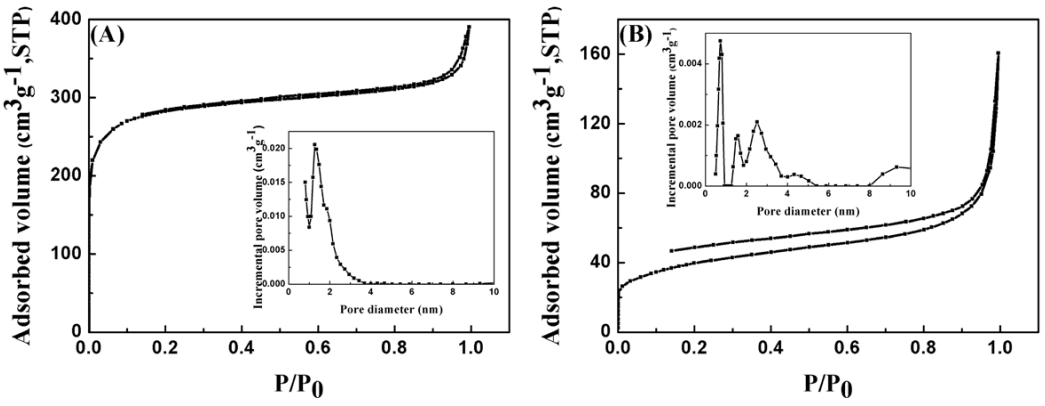


**Fig. 4**

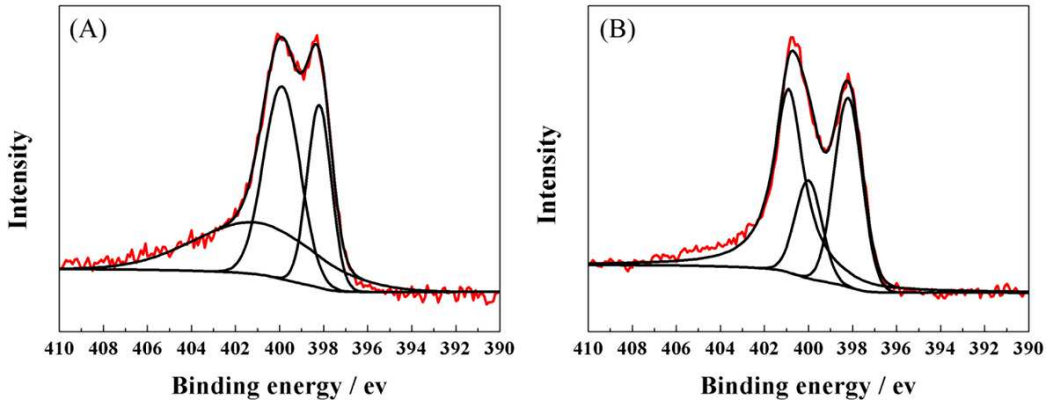


**Fig .5**

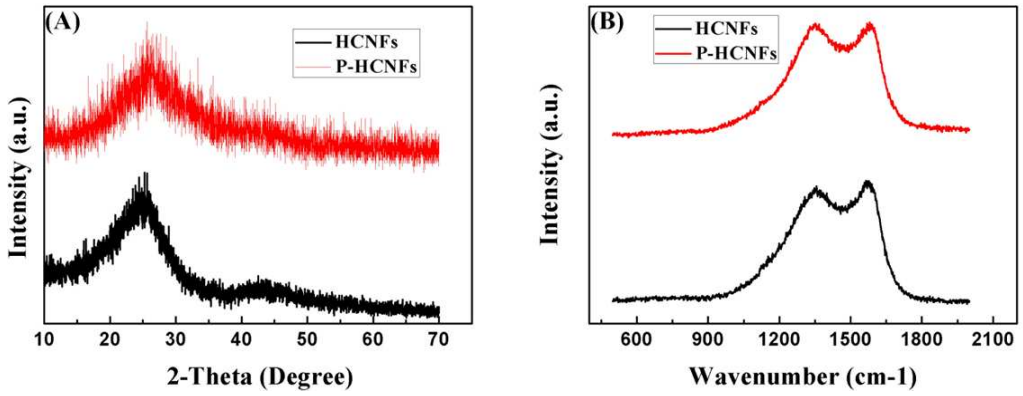


**Fig. 6**

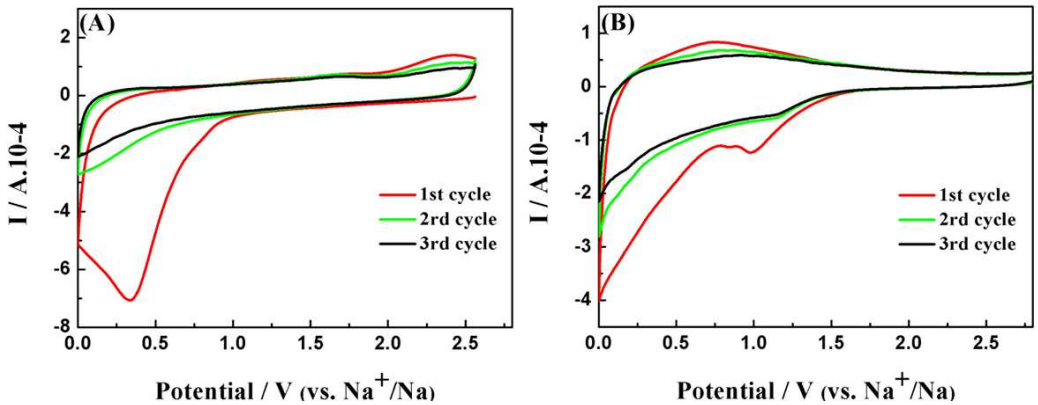


**Fig. 7**

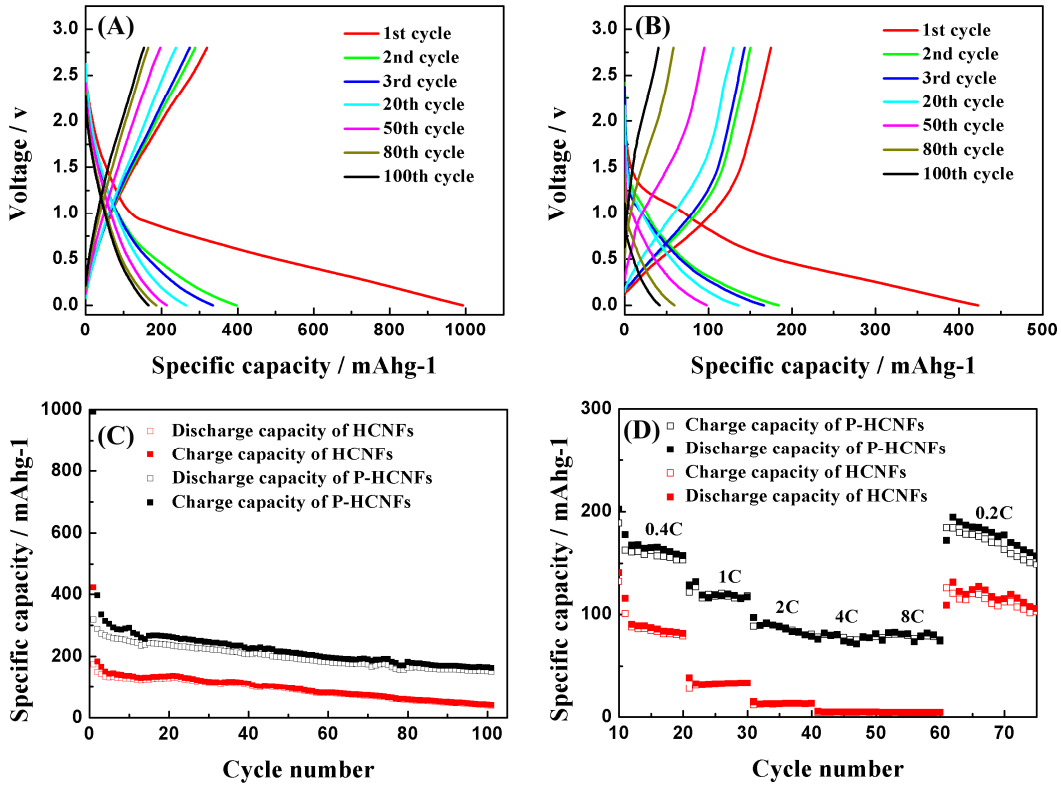


**Fig. 8**